Modelling and Control of the 18O Isotope Separation Plant

Marius Fișcă* Mihail Abrudean* Vlad Mureșan* Mihaela-Ligia Ungureșan Iulia Clitan* Roxana Cordoș *** Cristina Stăncioi***

** Automation Department, Technical University of Cluj-Napoca, 28 Memorandumului Street, 400114 Cluj-Napoca, Romania (e-mail: mariusfisca@gmail.com, mihai.abrudean@aut.utcluj.ro, vlad.muresan@aut.utcluj.ro, iulia.clitan@aut.utcluj.ro, stancioi_cristina@yahoo.com)*

*** Physics and Chemistry Department, Technical University of Cluj-Napoca, 28 Memorandumului Street, 400114 Cluj-Napoca, Romania (e-mail: mihaela.unguresan@chem.utcluj.ro)*

**** Management and Economic Engineering Department, Technical University of Cluj-Napoca, 28 Memorandumului Street, 400114 Cluj-Napoca, Romania (e-mail: roxana.cordos@mis.utcluj.ro)*

Abstract: The presented research results focus on modelling and control of the operation of a productive plant used for the ^{18}O isotope separation. The proposed mathematical model which describes the separation plant operation is based on using two strong nonlinear differential equations. To determine the separation process structure parameters, the available experimental data are processed. In the modelling procedure, the interdependency between the operations of the two separation columns from the separation plant structure is considered, too. The behaviour of the nonlinear structure parameters associated to the proposed model is learned using neural networks. The proposed control strategy for the ^{18}O isotope concentration at the output of the separation plant is based on the design of two controllers with complex structure, one for each of the two separation columns of the separation plant, controllers which integrate a model-based solution. The high performances of the proposed control strategy are proven through simulation, the simulations results being presented and interpreted in the final part sections of the manuscript. The previously mentioned high performances are obtained in the context of maintaining all the intermediary signals from the operation of the designed control systems between their imposed variation limits, aspect which makes feasible the proposed control solution for the practical implementation.

Keywords: modelling, simulation, control, ^{18}O isotope, separation cascade, neural networks, fractional-order model, experimental results.

1. INTRODUCTION

Stable isotopes present a great interest as tagging elements, being an extremely useful tool in a series of domains such as: energy, chemistry, biology, medicine and agriculture. The ^{18}O isotope can be used for positron emission tomography, respiratory tests in medicine, or as a tracer agent in the efficient usage of chemical fertilizers in agriculture (Branka & Beno, 2023; David et al., 2021; Reza & Mohamad, 2022). The most common methods of separating stable isotopes use distillation processes and counter current isotopic exchange in separation columns. The separation columns have, at the two ends, reflux systems that ensure a recirculation flux of the isotope separated from the liquid phase to the gas phase (in the lower part of the columns), respectively from the gas phase to the liquid phase (in the upper part of the columns) in order to ensure a continuous process. Experience accumulated in design, construction and experimentation of a laboratory intended installation for the enrichment of the heavy isotope of oxygen ^{18}O by counter current isotopic exchange on columns filled with nitrogen oxides and 4-8 mol/l nitric acid solution allowed the design of a productive installation for this isotope. Nitrogen oxides are used as feed as isotopic waste of the production plant for the separation of the heavy isotope of nitrogen ^{15}N. The installation used for ^{18}O separation by isotopic exchange in nitrogen oxides-water, nitric acid is presented in Fig. 1 (CI, CII – separation columns; 1, 2 – nitrogen oxide compressors; 3, 4 – flowmeters; 5, 6 – electric arc cracking reactor; 7, 8 – absorption for NOx in H_2O; 9, 10 – NOx preheating furnaces; 11, 13 – NO with H_2 conversion reactors; 12, 14 – NH_3 cracking reactors; 15-18 – heat exchangers; 19–22, 29, 30 – coolants; 23, 24, 31, 32 – molecular sieve absorption; 24-27, 33-36 – electromagnetic valves; 37–39 – absorbers for CO_2 purification; 40 – sodium hydroxide recuperator).

The use of nitrogen oxides that leave the ^{15}N production plant as waste ensures a low-cost price for ^{18}O production. This has a natural concentration equal to 0.204%^{18}O. Their prior purification is necessary so that CO_2 or other impurities that contain oxygen in their molecule do not enter the separation installation, which would dilute the concentration of heavy oxygen in the column, worsening the separation performance and prolonging the time of the transient regime to reach the maximum concentration and start the extraction in production regime. The CI column with an inner diameter of 50 mm has a height of 10 m, being composed of four sections assembled by a flange and teflon gasket. It is thermostated with water at 25°C in a closed circuit. The column filling is Helipak type, 2.5×2.5×0.2 mm, made of stainless-steel wire in the shape of

a twisted prism. Column CII has the same height, with an internal diameter of 16 mm, being provided with a thermostatic jacket with water at 25°C. It has the same type of filling as CI, with the size 1.8×1.8×0.2 mm (Axente et al., 1994; Abrudean, 1981).

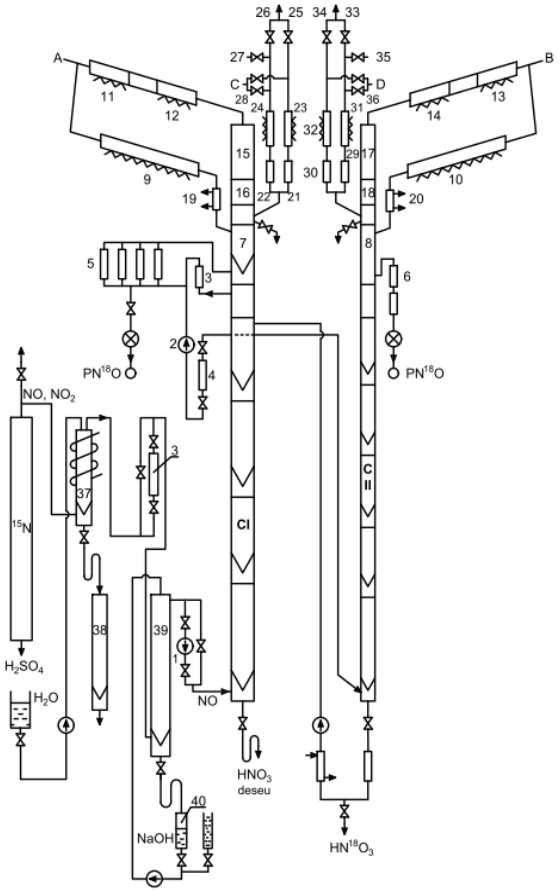

Figure 1. Installation for ^{18}O production

The separation columns have at the upper enrichment ends, complex reflux systems, which have the role of returning the isotope of interest (^{18}O) to the column, in the form of the aqueous solution of nitric acid 6-8 mol/l, and to create the liquid phase which flows in the column in counter current with nitrogen oxides. Malfunctioning of the equipment that makes up the total oxygen reflux system from the nitrogen oxides as the gaseous phase in aqueous nitric acid solution leads to the deterioration in performance of the separation of the isotope of interest, lowering its final concentration and implicitly the production on the separation cascades. The final enrichment column is fed with the product enriched in ^{18}O, in the form of ^{18}NOx with the help of a compressor for corrosive gases (Wolfram, 2017; Savarino & Thiemes, 1999). The gaseous phase from the upper ends of the separation columns is directed to the electric arc decomposition reactors, in number of four, for column CI and one for CII.

The sections at the ends of the separation columns are provided with a liquid guard which causes the gas phase to be completely diverted through the arc reactors. Electric arc cracking reactors (5, 6) are fed in parallel with nitrogen oxides, directly between their platinum electrodes. They work at high voltage and current intensity generating continuous electric arcing. They are made of temperature-resistant glass and have a double mass through which water circulates at 25°C, having the role of dissipating the heat resulting from the cracking of nitric oxide, obtaining nitrogen N_2 and atomic oxygen O_2. Atomic oxygen reacts quickly with nitric oxide NO that did not enter the area of the electric arc, resulting in nitrogen dioxide NO_2. Increasing the intensity of the electric arc leads to an increase in the amount of NO_2 in the gases leaving the arc reactors. Nitrogen dioxide absorbers (7, 8) have the role of forming the nitric acid solution. Nitrogen oxide enters the preheating furnaces (9, 10), and the water resulting from the conversion of NO with H_2 flows through the guard into the absorber where it will react with NO_2 and produce the nitric acid HNO_3. The reaction in the absorbers of the two columns being exothermic, thermostatic jackets with water at 25°C were provided, connected to the thermostatic separation columns. Thus, the heat released following the nitric acid formation reactions is dissipated, and the nitric acid solution flowing in the separation column has a temperature of 25°C. The nitric oxide leaving the absorbers passes through the preheating furnaces and then enters the conversion reactors (11, 13). In the conversion reactors nitric oxide reacts with excess hydrogen resulting water and ammonia. The ammonia resulting from these reactions is decomposed at 900-950°C in the cracking reactors (12) and (14), into nitrogen and hydrogen, being an unwanted by-product in this process of separating the ^{18}O isotope.

Hydrogen produced by the electrolysis of water contains traces of oxygen that dilute the concentration of ^{18}O in the reflux system of the isotopic separation columns, therefore it is catalytically purified beforehand from traces of oxygen by burning it, on palladium catalyst and recovering the water on the molecular sieve tower. Gases leaving the catalytic conversion reactors contain H_2O, H_2, N_2 and traces of NH_3. Condensation of the water is carried out in the heat exchangers (15) and (17), cooled with industrial water. The second condensation phase takes place in the heat exchangers (16) and (18), cooled to 0.25°C by recirculating an ethylene glycol-water mixture from a cooling station. The water guard located above the absorbers (7) and (8) allows the separation of the liquid circuit from the gas circuit, which passes through the heat exchangers (21), (22), (29) and (30), cooled to 0.25°C, molecular sieve adsorbers (23), (24), (31), (32) and is released into the atmosphere through the electromagnetic valve system. Purified and dried hydrogen is also used to regenerate molecular sieve absorbers. Hydrogen that feeds the catalytic reactors of the ^{18}O separation plant is obtained from cylinders under pressure (130 atm).

This are connected to a collector ramp (41), Fig. 2, built according to anti-explosive and pressure installations standards (where 41 – collector ramp for pressurized hydrogen cylinders; 42, 44, 47 – valve systems; 43 – medium pressure tank; 45 – low pressure tank; 46 – pressure gauges; 48 – molecular sieve absorbers; 49 – reactor with platinum catalyst on silica gel; 50 – heat exchanger; 51, 52 – molecular sieve adsorbers). The hydrogen supply system is equipped with two pressure regulators (42), mounted in parallel, which connect to the medium pressure tank (43) equipped with a EX-certified pressure gauge for pressure control and two safety valves set

at 4 atm. By means of an explosion proof solenoid valve (44) the connection to the low-pressure tank is made. Hydrogen from this tank passes through a flow regulator (47) and is directed through molecular sieve adsorbers (48) where water and other impurities from the supply cylinders are retained. In the reactor (49) oxygen and chlorine, as impurities from the cylinders react with hydrogen to form water and hydrochloric acid, which are retained on molecular sieve adsorbers (51) and (52).

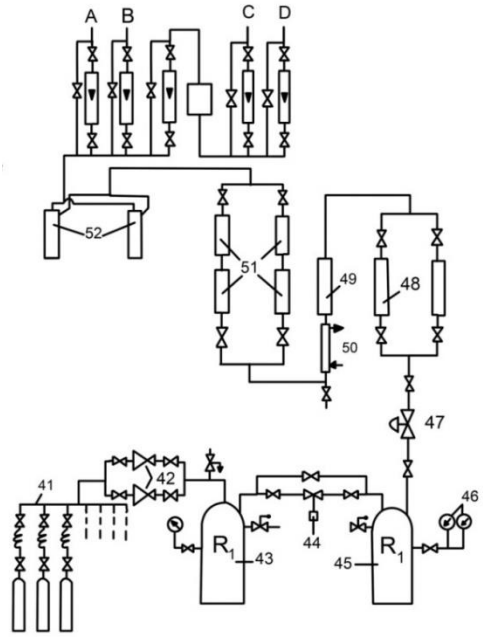

Figure 2. Hydrogen supply installation for ^{18}O obtaining process

The hydrogen, rising through flowmeters A and B, enters the conversion reactors (11) and (13) and the one rising through C and D enters molecular sieve adsorbers for its regeneration, therefor enters the ^{18}O production installation described in Fig. 1. The production installation for the separation of the ^{18}O isotope involves a slow, non-linear process, with a time constant of hundreds of hours and with a transient regime, upon commissioning, requiring between 20 and 30 days (Morin et al., 2011). Such a production facility requires working with toxic, corrosive, and explosive substances, its operation is continuously supervised and monitored by specialized operators. Malfunction of the separation process can compromise the production and ^{18}O concentration and involves the need to restart the separation process from the natural concentration of 0.204%^{18}O (E Kerstel et al., 1999).

Information obtained through modelling, simulation and control of the separation process allows the selection of the main operating parameters such as nitrogen and hydrogen oxide flow rates, loading of the separation columns (flow ratio/cross-sectional area of the columns), concentration of nitric acid solution in the column, temperature for preheating furnaces, conversion and cracking reactors and working pressure, for optimal process and production system operation.

2. AVAILABLE EXPERIMENTAL DATA

The experimental data used in this research is obtained from a real separation plant used for the ^{18}O isotope separation. All available experimental data is obtained during the operation of the separation cascade in total reflux regime. The total reflux regime is characterized by the enrichment of the ^{18}O isotope in the separation plant, but without extracting the product from it. Practically, in total reflux regime, the ^{18}O isotope concentration is increased up to a certain imposed value, the separation plant being prepared for following procedures. The operation regime in which the product is extracted from the separation plant is not considered in this manuscript. Also, the processed experimental data are obtained both from experimental procedures organized within research activities and during the normal plant operation. A high importance parameter is the Height of Equivalent Theoretical Plate (HETP) associated to each of the two separation columns from the separation plant structure (in this case, the separation plant is based on a separation cascade containing the CI and CII separation columns). Also, the HETP parameter is a function of the input nitric oxides flow in the corresponding separation column (these two flows ensure the separation plant supply). The input nitric oxides flow in CI is notated with $F_I(t)$ and the input nitric oxides flow in CII is notated with $F_{II}(t)$. The variation of the two flows imply directly the variation of the ^{18}O isotope concentrations at the output of the two separation columns (the output of the two separation columns are considered their tops, from where the product can be extracted in the production regime; the two separation columns are equal as height, both having the height L= 1000 cm; however, as it was mentioned in the first section of the manuscript, the two separation columns differ through their diameter). The procedure of experimentally obtaining $HETP_I(F_I)$ (for CI) and $HETP_{II}(F_{II})$ (for CII) function values is as follows:

1. the separation columns are disconnected from the separation cascade and during the carrying out of the experiments they operate independently;
2. for each separation column, a constant input nitric oxides flow is applied at its input;
3. for both separation columns, each experiment is stopped only when the steady state regime is reached;
4. for both separation columns, the steady state values of the ^{18}O isotope concentration at their tops are measured and using the direct analytical dependency between the ^{18}O isotope steady state concentration and HETP, the $HETP_I(F_I)$ and $HETP_{II}(F_{II})$ functions values are determined;
5. the stages 2-4 are repeated for enough input nitric oxides flows to obtain valid dynamics for $HETP_I(F_I)$ and $HETP_{II}(F_{II})$.

Consequently, the experimental results for the two HETP functions are included in Table 1. From one experiment to the next, the advance step of ΔF_I= 100 l/h is applied in the case of CI, respectively the advance step of ΔF_{II} = 7.5 l/h is applied in the case of CII. From Table 1, it results that the two HETP functions variations are not monotonous. To analyse the dynamics of the two HETP functions in relation to the corresponding nitric oxides input flows, the graphical representations in Fig. 3 and Fig. 4 are required.

From Fig. 1 and 2, the fact that the HETP functions are nonlinear results, considering their entire definition domains.

However, the HETP functions have a linear variation on different variation domains of the corresponding nitric oxides flows. Also, based on the mathematical dependency between the HETP functions and the corresponding nitric oxides flows, for the minimum values of the graphs from Figs. 3 and 4, the ^{18}O isotope steady state concentrations at the output of the two separation columns have the maximum values. Consequently, the higher the values represented by the graphs are (Figs. 3 and 4), the lower the ^{18}O isotope steady state concentrations are, at the output of the two separation columns.

Other important experimental results are usable to determine the dynamics, in relation to time, of the ^{18}O isotope concentration at the outputs of the two separation columns. In this context, the open loop step responses of the CI and CII which take part from the separation cascade structure is of great interest.

Table 1. Experimental results for HETP functions

Nº	F_I [l/h]	$HETP_I(F_I)$ [cm]	F_{II} [l/h]	$HETP_{II}(F_{II})$ [cm]
1	770	13.148	60	14.998
2	870	12.521	67.5	14.399
3	970	11.894	75	13.8
4	1070	11.267	82.5	13.199
5	1170	10.64	90	12.599
6	1270	10.013	97.5	12
7	1370	9.385	105	11.399
8	1470	8.758	112.5	10.8
9	1570	8.131	120	10.199
10	1670	7.505	127.5	9.6
11	1770	6.874	135	9
12	1870	6.997	142.5	8.682
13	1970	7.259	150	8.931
14	2070	7.521	157.5	9.183
15	2170	7.781	165	9.432
16	2270	8.042	172.5	9.682
17	2370	8.301	180	9.932

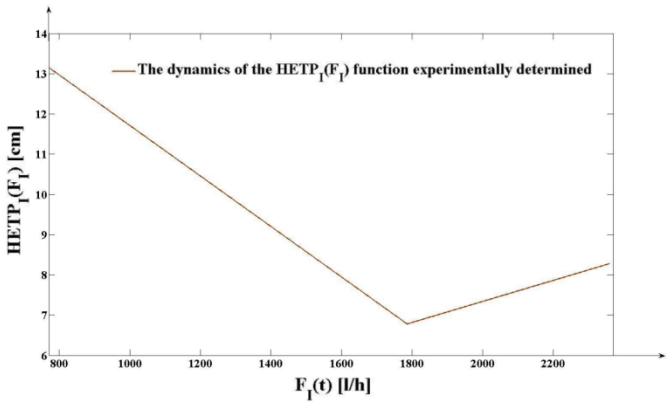

Figure 3. The $HETP_I(F_I)$ dynamics experimentally determined

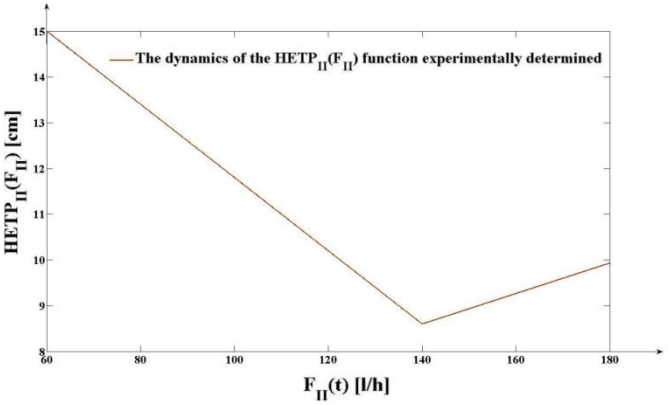

Figure 4. The HETPII(FII) dynamics experimentally determined

In Fig. 5, the open loop step responses of CI and CII (which form the separation cascade) are presented, in the case when the applied input nitric oxides flow have the values $F_I = 880$ l/h and $F_{II} = 80$ l/h.

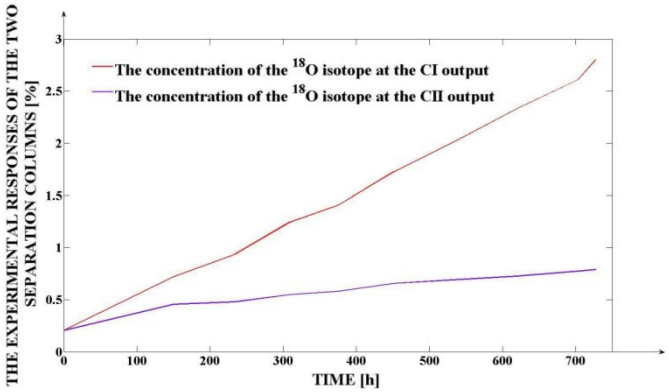

Figure 5. The step responses of CI and CII from the separation cascade structure

The experiment in which the two responses presented in Fig. 5 were determined, was stopped after 730 h from its start due to a malfunction that occurred in one of the separation plant equipment. Even if the steady state values of the ^{18}O isotope concentration at the two separation columns tops were not reached, the experimental curves presented in Fig. 5 have a long enough duration to be relevant for determining the dynamics in relation to time (the inertias) of CI and CII. From Fig. 5, it results that the approached separation process is an extremely slow one, having time constants of hundreds of hours. Consequently, the steady state regimes of the ^{18}O isotope concentrations at the CI and CII tops is reached in more than 1000 h. Also, the ^{18}O isotope concentration at the CII top has significantly higher values than the ^{18}O isotope concentration at the CI top, on the entire duration of the experiment, and the difference increases in relation to time. Obviously, the difference between the two values gets steady in steady state regime. These higher values are physically justified through the fact that CII separates the ^{18}O isotope already separated by CI (due to the fact that CI and CII are connected in a separation cascade structure).

The variations of the $T_I(F_I(t))$ and $T_{II}(F_{II}(t))$ functions, experimentally determined, is presented in Fig. 6. An element which implies a consistent nonlinearity in the separation plant

operation is the fact that the time constants of the two separation columns (one time constant for each separation column) present significant variations during the plant operation. Also, the time constants are functions depending on the two nitric oxides flows ($T_I(F_I(t))$ in case of CI and $T_{II}(F_{II}(t))$ in case of CII). To highlight both functions on the same graph, on the abscissa, F_I is expressed in l/h and F_{II} is expressed in dl/h (this have different order of magnitude). From Fig. 6, it results that the two functions are nonlinear. Also, the experimental values associated to the two curves presented in Fig. 6 were obtained by making measurements during the separation plant operation in different preliminary production regimes (as total reflux regimes) or in production regimes.

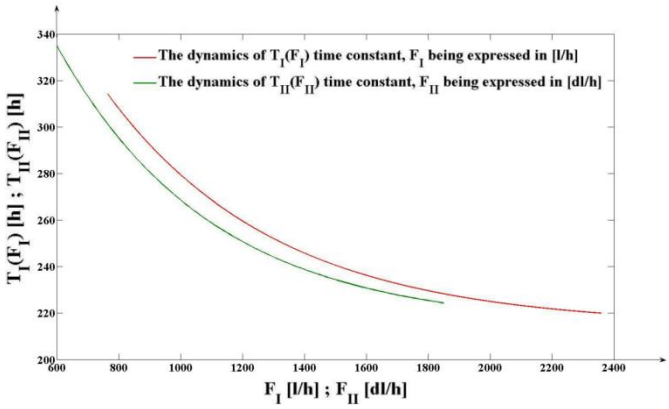

Figure 6. The dynamics of CI and CII time constants in relation to F_I, respectively to F_{II}

3. SEPARATION PLANT OPERATION MATHEMATICAL MODEL

The first stage in obtaining the mathematical model describing the separation plant operation is the approximation of the $T_I(F_I(t))$ and $HETP_I(F_I(t))$ functions, respectively of the $T_{II}(F_{II}(t))$ and $HETP_{II}(F_{II}(t))$ functions. Also, in the case of CII, another function FOCS(t) (Fractional Order Compensation Signal) must be approximated. Details about this function will be given later in this section. To obtain compact approximation entities for these functions and in order to obtain the highest possible approximation accuracy, neural networks are used. In this context, the signals (functions) associated to each separation column are approached as group of signals (functions). Consequently, two feedforward connected neural networks (Chen et al., 2020) are used to learn the dynamics of each of the two group of signals.

In the case of CI, a feedforward connected neural network containing 17 nonlinear neurons (having bipolar sigmoid, hyperbolic tangent, activation functions) in the hidden layer (only one layer is defined) and 2 linear neurons in the output layer is used, the input signal being $F_I(t)$. The used learning algorithm is Levenberg-Marquardt (Muresan et al. 2015) and the maximum number of epochs was set at 45000. As quality indicator, the Mean Square Error (MSE), is used. The imposed MSE target value represents the value for which the correlation coefficients between the values of both output signals generated by the neural network and the corresponding experimental values are minimum 99%. As training data, pairs of input-output experimental data presented in Fig. 3 and in Fig. 6 (case of the red curve) are used. By applying the training procedure, the target MSE was obtained after 41324 epochs. According to the equation associated to the neural network, the two output signals $T_I(F_I(t))$ and $HETP_I(F_I(t))$ are given by (1):

$$\begin{pmatrix} T_I(F_I(t)) \\ HETP_I(F_I(t)) \end{pmatrix} = W_{ILAY} \cdot sig(W_{Ii} \cdot F_I(t) + B_{ILAY}) + B_{IOUT} \quad (1)$$

where $W_{Ii}[17\times1]$ is the solution vector which contains the solution input weights (obtained after applying the training procedure), $B_{ILAY}[17\times1]$ is the solution vector which contains the solution bias values of the neurons from the hidden layer, $W_{ILAY}[2\times17]$ is the solution matrix which contains the solution weights that connect the neurons from the hidden layer with the two neurons from the output layer, $B_{IOUT}[2\times1]$ is the solution vector which contains the solution bias values of the neurons from the output layer and the notation "sig" is referring to the application of the bipolar sigmoid activation function.

In case of CII, a similar procedure is applied. The same structure of neural network is used but having 24 nonlinear neurons in the hidden layer and 3 linear neurons in the output layer (this neural network approximates three functions). Also, the same learning algorithm and quality indicator are used. The maximum number of epochs is set to 70000 and the target MSE is obtained after 61387 epochs. As training data, pairs of input-output experimental data presented in Fig. 4 and 6 (he green curve), respectively data associated to the FOCS(t) output signal are used. According to the equation associated to the second neural network, the three output signals $T_{II}(F_{II}(t))$ and $HETP_{II}(F_{II}(t))$ and FOCS(t) are given by (2):

$$\begin{pmatrix} T_{II}(F_{II}(t)) \\ HETP_{II}(F_{II}(t)) \end{pmatrix} = W_{IILAY} \cdot sig(W_{IIi} \cdot F_{II}(t) + B_{IILAY}) + B_{IIOUT} \quad (2)$$

where $W_{IIi}[24\times1]$, $B_{IILAY}[24\times1]$, $W_{IILAY}[3\times24]$, $B_{IIOUT}[3\times1]$ and the notation "sig" have the same significance as in previous case.

Having the signals given by (1) and (2), the next stage of modelling can be implemented. Consequently, the system of four equations (3)-(6) which describe the dynamics of the separation plant in relation to time, is:

$$T_I(F_I(t)) \cdot D_t^1(C_{IONA}(t)) + C_{IONA}(t) = C_0 \cdot \left(\alpha^{\frac{L}{HETP_I(F_I(t))}} - 1 \right) \quad (3)$$

$$C_I(t) = C_{IONA}(t) + C_0 \quad (4)$$

$$T_{II}(F_{II}(t)) \cdot D_t^{\mu}(C_{IIONA}(t)) + C_{IIONA}(t) = C_I(t) \cdot \alpha^{\frac{L}{HETP_{II}(F_{II}(t))}} - C_0 \quad (5)$$

$$C_{II}(t) = C_{IIONA}(t) \cdot FOCS(t) + C_0 \quad (6)$$

This system of equations contains two nonlinear differential equations (3) and (5) and two algebraic equations (4) and (6). Also, (5) is a fractional-order differential equation. In (3)-(6), C_0= 0.204% represents the natural abundance (natural concentration) of the ^{18}O isotope, respectively in (3) and (5), α= 1.018 [-] represents the elementary separation factor of the

^{18}O isotope. (3) models the dynamics of CI separation column. The signal $C_{IONA}(t)$ signifies the concentration of the ^{18}O isotope, at the CI top, over the C_0 value. The notation D_t^1 highlights the first order derivative in relation to time of the brackets represented signal. Also, the term $SEP_I(t) = \alpha^{\frac{L}{HETP_I(F_I(t))}}$ represents a signal called the CI separation. The concentration of the ^{18}O isotope at the CI top is notated with $C_I(t)$ and it is given by (4). In (5), the notation D_t^μ highlights the fractional-order derivative of μ order of the represented signal (μ represents the fractional differentiation order). Also, the $C_{IIONA}(t)$ signal signifies the concentration of the ^{18}O isotope, at the CII top, over the C_0 value. The term $SEP_{II}(t) = \alpha^{\frac{L}{HETP_{II}(F_{II}(t))}}$ represents the CII separation. Finally, the concentration of the ^{18}O isotope concentration at the CII top is notated with $C_{II}(t)$ and it is given by (6). Since the $T_I(F_I(t))$, $HETP_I(F_I(t))$, $T_{II}(F_{II}(t))$, $HETP_{II}(F_{II}(t))$ and FOCS(t) functions are given by the two previously presented neural networks (forward referred to as NMI and NMII), the parameter which remains to be determined is μ. To identify the fractional differentiation order, the (3)-(6) equations are singularized considering the values F_I = 880 l/h and F_{II} = 80 l/h for the two input nitric oxides flows (the values used in the case of the experimental procedures in which the responses from Fig. 5 are determined). According to Fig. 6, for these nitric oxides flows values, the separation plant time constants are T_I = 210 h and T_{II} = 295 h. Considering the singularized time constants values, the μ differentiation order is determined iteratively. In this context, the μ differentiation order is initialized to the value 0.7 and the corresponding advance step is fixed at the value $\Delta\mu$= 0.02. The proposed model is simulated iteratively for all the values of μ between 0.7 and 1, respecting the mentioned advance step. In each simulation case, the MSE value between the experimental response of CII presented in Fig. 5 and the simulated response is computed, for the interval of time in which the experimental data are available. After finishing all the simulations, the μ differentiation order for which the smallest MSE value is obtained is declared the identification solution. After applying this algorithm, the value μ= 0.92 results. In case of CI, the same procedure could be applied to improve the model accuracy. However, after a consistent analysis, the accuracy improves in the case of using a fractional-order model for CI, too, is insignificant and consequently the implementation of such a solution is not justified due to its complexity. For this reason, in (3), $D_t^\alpha() = D_t^1()$ is used.

In Fig. 7, the comparative graph between the experimental response of CII and the simulated response of the proposed fractional-order model is presented. Also, in this figure, the response of the alternative integer-order model, obtained by imposing μ= 1 in (5) and by making the corresponding adjustments, is also presented. All three responses apply for the same hypothesis in which the input nitric oxides flows are step type signals, having the steady state values F_I = 880 l/h and F_{II} = 80 l/h. From Fig. 7 it results a consistently better superposition between the red curve (representing the response of the proposed fractional-order mathematical model) and the experimental response (highlighted with blue colour) than in the case of the alternative integer-order model.

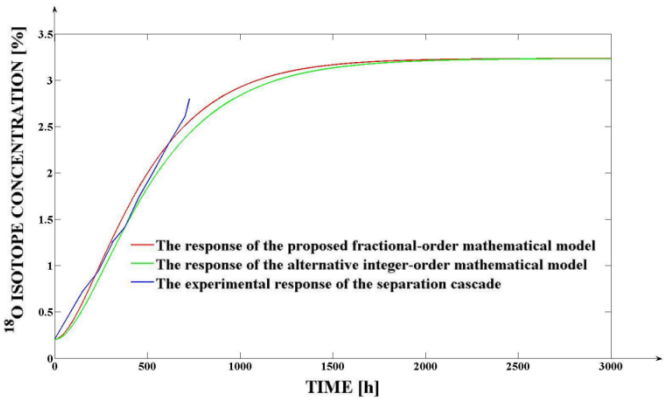

Figure 7. The comparison between the experimental response of CII and the responses of the two proposed possible mathematical models

Practically, the red curve "averages" much better the data associated to the experimental response. Consequently, the conclusion that the proposed fractional-order model is an efficient one results, and it will be used further in this manuscript to implement the control strategy of the ^{18}O isotope concentration value. Also, from Fig. 7, it results that the most probably steady state value of the experimental response is CII_{st} = 3.2338%, being given by the steady state value of the proposed fractional-order mathematical model presented in this figure, too. The FOCS(t) function is necessary to be used in order to compensate the deviation of the steady state value of the CII mathematical model response due to the fact that it is a fractional-order one.

The compensation can be computed based on the final value theorem applied to the Oustaloup approximations of the fractional order transfer functions resulted by singularizing (5) for different values of the $F_{II}(t)$ nitric oxides input flow. Practically the compensation is given by the inverse ratio between the free coefficients of the numerator, respectively of the denominator from the Oustaloup approximation structure. Obviously, different values of $F_{II}(t)$ being used (covering its entire variation domain), different values of the FOCS(t) function are determined and the associated training data NMII are obtained.

4. PROPOSED CONTROL STRATEGY FOR ^{18}O ISOTOPE CONCENTRATION

The proposed control strategy for the most important output parameter (signal) of the separation plant, more exactly the ^{18}O isotope concentration, is implemented using the control structure presented in Fig. 8. To introduce the notations used in Fig. 8, the convention that if the defined element or signal contains the letter "I" it is associated to the first separation column and if the defined element or signal contains the letters "II" consecutively written it is associated to the second separation column from the separation cascade structure, is implied. Otherwise, the notations are similar. In this context, the following notations are used: SPC – Separation Process associated to the Column; P – Pump; FM – Flowmeter; CS – Concentration Sensor (for the ^{18}O isotope); CMBCC – Complex Model Based Concentration Controller; FA – Fault Analyzer; $C_{SP}(t)$ – Concentration Set-Point signal; C(t) – ^{18}O

isotope Output Concentration (Output Signal from the Separation Column and from the control system); $C_f(t)$ – Feedback signal proportionally with the ^{18}O isotope Concentration (feedback signal generated by the CS element); F(t) – the input nitric oxides Flow in the separation column; cs(t) – Control Signal; cs_{max}– the maximum value of the Control Signal which implies the maximum input nitric oxides flow; $cs_i(t)$ – initial Control Signal (the control signal generated directly by CMBCC); $a_C(t)$ – error signal for concentration; $F_m(t)$ – the measured Flow (the feedback signal generated by FM) $d_P(t)$ – disturbance signal which perturbs the operation of the pump; $d_C(t)$ – disturbance signal which perturbs the operation of the separation column; DECISION – decision generated by FA after analysing the $C_f(t)$ signal value.

In both separation columns cases, the error signals and the control signals can be expressed as the difference between the two concentration and control signal values, as follows:

$$a_C(t)=C_{SP}(t)-C_f(t) \quad (7)$$

$$s(t)=cs_{max}(t)-cs_i(t) \quad (8)$$

In (8) it is highlighted that the initial control signal $cs_i(t)$ generated by CMBCC represents the value which has to be subtracted from cs_{max} to obtain the final control signal cs(t). Using this strategy, the drying phenomenon of two columns is avoided. In most cases, the effects of disturbances imply the decrease of the output ^{18}O isotope concentrations from the two separation columns (Barkan & Luz, 2003). The interconnection between the two separation columns which defines their usage in a separation cascade structure, is highlighted in Fig. 8 by the transmission of the $C_I(t)$ signal from the first control system to the SPCII. Physically, this connection signifies, as previously mentioned, that CII separates the ^{18}O isotope already separated by CI. In other words, $C_I(t)$ represents, also, an input signal in CII. As an important remark, the electronic circuits which process the values of the two cs(t) signals and which imply the speed variations of the two pumps and implicitly the variations of the two columns nitric oxides input flows are included in the structures of the P elements from Fig. 8. The two control systems from Fig. 8 are at the base negative feedback structures but containing, each, a complex concentration controller. As it is highlighted in Fig. 8, the two complex controllers process, each, four input signals ($a_C(t)$, $C_f(t)$, $F_m(t)$ and cs(t)) to obtain the $cs_i(t)$ control signal.

The DECISION signals are taken by the FA elements after analysing the instantaneous values of the deviations of the $C_f(t)$ signals in relation to their usually average statistic values. In case when the deviations increases after a certain predefined value, the presence of a fault in the system is detected. Consequently, the decision can be the stop of the separation plant operation, in case a major fault occurs, or the continuous operation of the separation plant in fault rejection mode, in case a minor fault occurs. The fault quantification is established in relation to the previously mentioned deviations of the $C_f(t)$ signals values. To describe the structures of the CMBCC elements, the case of the CMBCCII is considered. Colours are used as follows: the purple arrows highlight input signals in the controller, the red arrow signifies the output signal from the controller and the blue arrows signify the internal signals of the controller. The complexity of the two controllers is justified due to the two separation processes complexity (nonlinear processes, fractional-order process in case of CII, extremely slow processes – these aspects give the characteristic of nonconventional processes). In this context, the CMBCCII structure is presented in Fig. 9 (where MPII

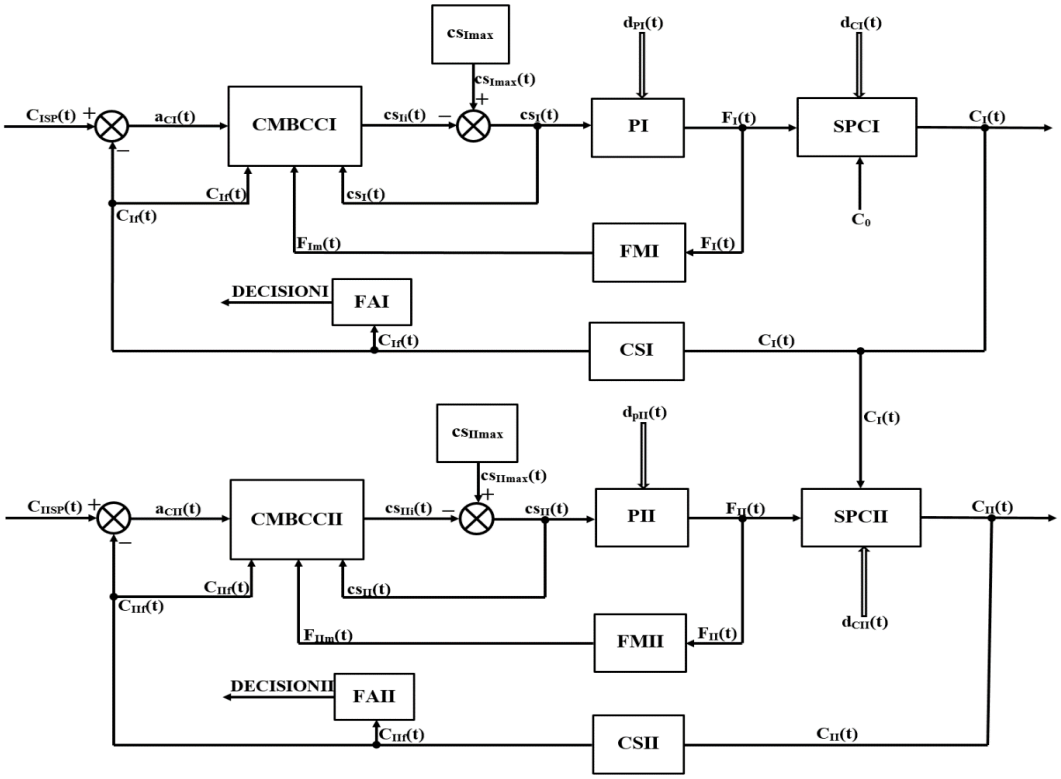

Figure 8. Proposed control structure for ^{18}O concentration

represents the mathematical model which describes the operation of the pump PII). The PII can be modelled as a first order linear process. Consequently, to implement the PII mathematical model, a first order equation with difference is used. Using MPII, the controller input signal $cs_{II}(t)$ is used for approximating the $F_{SII}(t)$ signal which signifies the simulated value of the $F_{II}(t)$ input nitric oxides flow. This signal is further necessary for simulating the separation process associated to CII. The NMII neural network has been presented, in detail, in the previous section of the manuscript, where it was used to generate the $T_{II}(F_{II}(t))$, $HETP_{II}(F_{II}(t))$ and FOCS(t) functions. The input signal in the controller which is, also, applied at the NMII input is $F_{IIm}(t)$ (the measured value of the $F_{II}(t)$ input nitric oxides flow) (K Pathiratne & R Lovett, 2016).

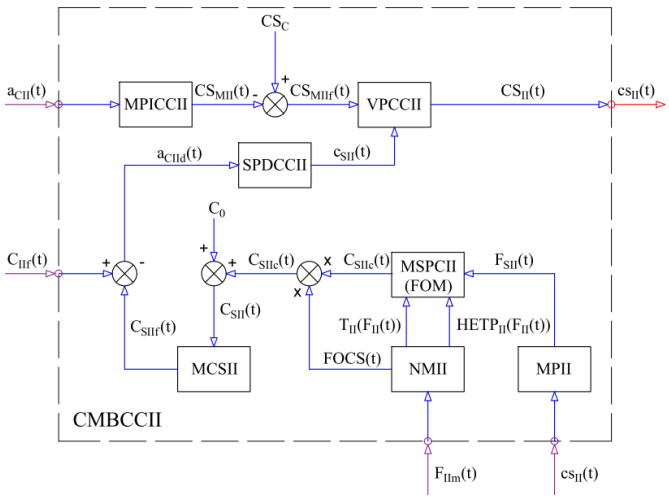

Figure 9. CMBCCII structure

In the controller structure, MSPCII represents the Model of the Separation Process associated to the second separation column CII which is a Fractional-Order Model (FOM). The implementation of MSPCII (FOM) element is presented in Fig. 10.

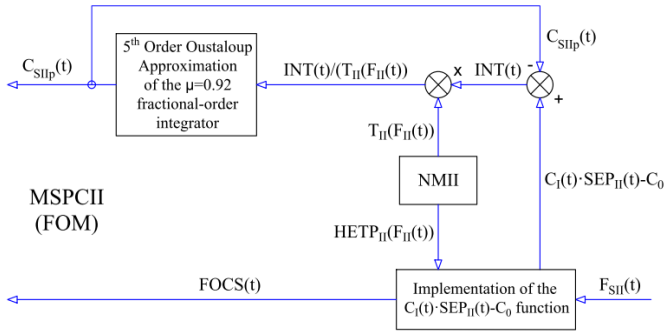

Figure 10. Implementation of MSPCII (FOM)

Practically, the implementation of MSPCII (FOM) is based on (5). Firstly, the $(C_I(t)\cdot SEP_{II}(t) - C_0)$ function is implemented according to the right member of (5). The output signal from MSPCII is $C_{SIIp}(t)$ (primary form of the simulated ^{18}O isotope concentration at the CII top) which is the simulated form of $C_{IIONA}(t)$ signal. The intermediary signal INT(t) is expressed as the following equation:

$$INT(t)=(C_I(t)\cdot SEP_{II}-C_0)-C_{SIIp}(t) \quad (9)$$

Also, the effect of the CII time constant is introduced by dividing the intermediary signal previously defined to $T_{II}(F_{II}(t))$ function $(INT(t)/(T_{II}(F_{II}(t))))$. The $\mu = 0.92$ fractional-order integrator is implemented using the Oustaloup approximation of 5th order, which has the form:

$$\frac{1}{s^{\mu}} \approx \sum_{i=5}^{0} \frac{d_i \cdot s^i}{e_i \cdot s^i} \quad (10)$$

where d_i ($i \in \{0, 1, 2, 3, 4, 5\}$ are the coefficients of the Oustaloup approximation numerator and e_i ($i \in \{0, 1, 2, 3, 4, 5\}$ are the coefficients of the Oustaloup approximation denominator.

Next, (6) is implemented to obtain consecutively, the corrected form of the $C_{SIIp}(t)$ signal ($C_{SIIc}(t)$) - by applying the FOCS(t) and the simulated ^{18}O isotope concentration at the CII top ($C_{SII}(t)$). The notation MCSII referred to the Model of the Concentration Sensor which is used for measuring the ^{18}O isotope concentration at the CII output. As in case of MPII, in order to express the CSII model, a first order equation with difference is used. At the MCSII output, the simulated feedback signal proportional with the ^{18}O isotope concentration at the CII top is generated ($C_{SIIf}(t)$). By subtracting $C_{SIIf}(t)$ from $C_{IIf}(t)$ (which is, also, an input signal in the complex controller), the simulated error $a_{CIId}(t)$ is obtained. This error is a measure of all types of disturbances which occur in the CII operation (both exogenous and parametric disturbances). CMBCCII is a model-based controller since models of the elements from the control system are used in order to implement the proposed control strategy. The main error signal $a_{CII}(t)$ is, also, an input signal in the complex controller and it is processed by MPICCII (Main Proportional-Integral (PI) ^{18}O isotope Concentration Controller at the CII top). The transfer function of MPICCII is given by:

$$H_{MPICCII}(s)=\frac{K_{PII}\cdot s+K_{III}}{s} \quad (11)$$

where K_{PII} is the proportionality constant of the MPICCII and K_{III} is the integral constant of the controller ($K_{III} = K_{PII}/T_{II}$, T_{II} being the integral time constant of the MPICIII). The MPICCII generates at the output the main control signal $cs_{MII}(t)$ which is subtracted from the constant component of the control signal cs_C. The final main control signal is given by:

$$cs_{MIIf}(t) = cs_C - cs_{MII}(t) \quad (12)$$

The parameters of the MPICCII are tuned using the relay method associated to the Ziegler-Nichols equations. The integral component of MPICCII ensures null error for the output ^{18}O isotope concentration. Also, the usage of cs_C signal ensures the avoidance of the CII separation plant start at the maximum nitric oxides input flow (this risk occurs without using cs_C due to the usage of $cs_{max}(t)$).

The SPDCCII (Secondary Proportional-Derivative (PD) ^{18}O isotope Concentration Controller at the CII top) processes the

$a_{CIId}(t)$ error signal and generates the output secondary control signal $cs_{SII}(t)$. The transfer function of SPDCCII is given by:

$$H_{SPDCCII}(s)=\frac{K_{DII}\cdot s+K_{PPDII}}{T_{fII}\cdot s+1} \qquad (13)$$

where K_{PPDII} is the proportionality constant of the SPDCCII, K_{DII} is the derivative constant of SPDCCII ($K_{DII} = K_{PPDII}\cdot T_{DII}$, T_{DII} being the derivative time constant of SPDCCII) and T_{fII} is the time constant of the first order filter which is used to obtain the feasible form of the SPDCCII.

The SPDCCII is tuned using the principle of the compensation of the dominant time constant of the separation process associated to CII ($T_{II}(F_{II}(t))$. The SPDCCII is used to obtain a faster dynamic for the closed loop control system. The VPCCII (Variable Proportionality Constant of the Controller II) is an element which implements the following equation:

$$cs_{II}(t) = K_{VP}\cdot cs_{SII}(t)\cdot cs_{MIIf}(t) \qquad (14)$$

where $K_{VPP}(t) = K_{VP}\cdot cs_{SII}(t)$ is the variable proportionality constant of the complex controller (K_{VP} being its constant component, more exactly a weighting coefficient). The K_{VP} weighting coefficient is tuned to avoid the $cs_{II}(t)$ control signal saturation. Also, $cs_{II}(t)$ is the control signal generated by CMBCCII, more exactly its output signal (equivalent with $cs_{IIi}(t)$ from Fig. 8). Due to the $K_{VPP}(t)$ variation, the CMBCCII has the property of being an adaptive controller (Monje et al., 2010).

In the case of CMBCCI, all the explanations are the same as in the case of CMBCCII, but with the following differences: the FOCS(t) signal is no longer necessary due to the fact that the separation process associated to CI is not a fractional-order one; in the case of MSPCI implementation, due to the fact that $\mu = 1$, the Oustaloup approximation is no more necessary; all the elements and signals from Figs. 9 and 10 have to be singularized for the CI case; the parameters of the controllers from (11), (13) and (14) have to be singularized for the case of CI (their tunings generate different coefficients than in the case of CII).

5. RESULTS OF THE SIMULATION

The proposed control structure from Fig. 8 was implemented and simulated in MATLAB/ Simulink. Next, the simulations results are presented.

In Fig. 11, the comparative graph between the CI responses (obviously, considering the CI operation of the previously presented structure in the ^{18}O isotope separation cascade) in open loop regime and using the proposed control strategy, is presented. In case of using the proposed control system from Fig. 8, the set-point concentration was set to $C_{ISP}(t) = 1.25$ %. Also, in case of the open loop step response, the CI input nitric oxides flow was set to the final value $F_{I1} = 1297.5$ l/h, value previously computed and suited to obtain the CI top concentration of 1.25 % for the ^{18}O isotope. From Fig. 11, it results that, in both cases the imposed steady state value of the ^{18}O isotope concentration of 1.25 % is obtained and implicitly the steady state error of the response obtained in case of using the proposed control strategy in null ($a_{CIst} = 0$ %).

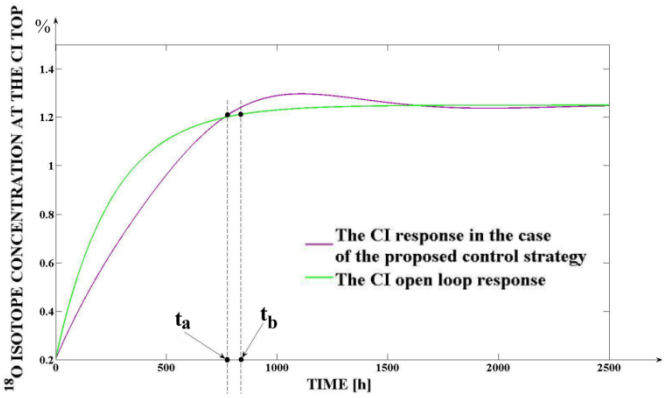

Figure 11. The comparative graph between the CI response, using the proposed control strategy and the CI open loop response

The first advantage of the proposed control strategy implementation is the fact that the appropriate input nitric oxides flow which ensures a certain imposed concentration at the CI output does not have to be anymore computed (these results as the effect of the control). The second advantage generated by the implementation of the proposed control strategy is referring to the main performance that has to be obtained, more exactly the settling time. Hence, imposing a steady state band of ±3.75 % near the steady state concentration value of the ^{18}O isotope at the CI output, the settling time $t_a = 766.5$ h is obtained in case of using the control system, respectively the settling time $t_b = 829.8$ h is obtained in case of the open loop response. Consequently, by using the proposed control system, the settling time is reduced with $\Delta t_1 = 63.3$ h. (representing a consistent improvement). The overshoot of the control system response from Fig. 11 has the value $\sigma_1 = 3.73$ %. The overshoot occurrence has not a negative influence on the separation cascade operation since the associated response value is enclosed in the previously imposed steady state band of ±3.75 %.

The comparative graph between the CII responses in open loop regime and in the case of using the proposed control strategy is presented in Fig. 12. For this simulation, the ^{18}O isotope concentration set-point value of $C_{IISP}(t) = 7$ % is imposed. For the open loop step response of CII, the input nitric oxides flow $F_{II1} = 118.11$ l/h is applied.

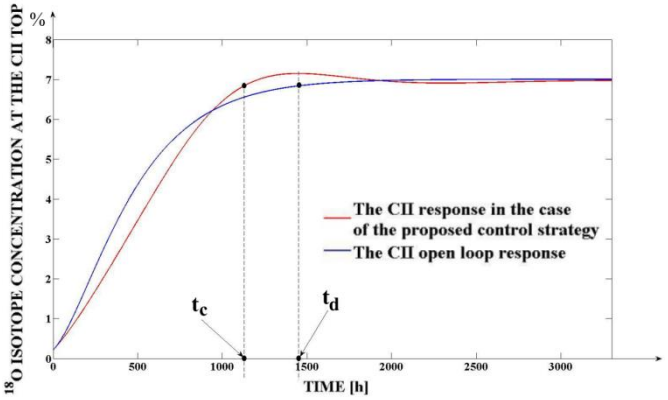

Figure 12. The comparative graph between the CII response, using the proposed control strategy and the CII open loop response

The imposed steady state band near the steady state value of the CII response is of ±2.25 %. By analysing Fig. 12, the same advantages of using the proposed control strategy as in case of CI are identified. In case of the settling time performance, the advantage is a major one, the control system generating the value $t_c = 1132.4$ h which is with $\Delta t_2 = 324.7$ h smaller than the value obtained in open loop regime, more exactly $t_d = 1457.1$ h. Practically, the product at the imposed concentration can be extracted with almost 2 weeks faster in case of implementing the proposed control systems from Fig. 8 than in the situation of using the separation cascade in open loop regime. The overshoot of the control system response from Fig. 12 has the value $\sigma_2 = 2.13$ %, the same conclusion as in the case of CI resulting.

The third advantage of implementing the proposed control strategy is its capacity of rejecting efficiently the effects of the disturbances which occur in the separation plant operation. In this context, in order to test the control system responses in disturbances effects rejecting regimes, two equivalent disturbances which modify directly the ^{18}O isotope concentrations at the CI and CII tops, having values which are consistently higher (in module) than the normal statistical ones (being of step types, these disturbances have null initial values and their steady state values, are: $d_{CI1} = -0.15$ % and $d_{CII1} = -1$ %; the commutation from the initial to their final values, corresponding to the disturbances occurrence in the system, takes place at the moment $t_{com} = 4000$ h from the simulation start; practically, the two disturbances occur simultaneously in the separation plant) (Savarino & Thiemens, 1999).

The responses of the two control systems from Fig. 8, in case when the mentioned disturbances occur in the separation plant operation, are presented comparatively with the open loop step responses of the associated separation columns (operating in the separation cascade structure type) in Figs. 13 and 14. In the cases of the open loop responses, the same input nitric oxides flows F_{I1} and F_{II1} as in the cases of the simulations from Figs. 11 and 12 are used. To analyse the settling times in rejecting regimes of the disturbance's effects, the same steady state bands as in the cases of the simulations presented in Figs. 11 and 12 are considered. From Fig. 13, it results that, in the case of the open loop response, the effect of d_{CI1} is not rejected and, due to the disturbance effect, the response of CI gets steady to the value of 1.1 %. Also, the CMBCCI rejects efficiently the effect of the d_{CI1} disturbance after $t_e = 862.2$ h from the moment of the disturbance occurrence (t_{com}). From Fig. 14, it results that the effect of d_{CII1} disturbance is not rejected in open loop operation regime, the corresponding response of CII getting steady to the value of 6 %. The CMBCCII rejects efficiently the effect of the d_{CII1} disturbance after $t_f = 1118.07$ h from the moment of its occurrence (t_{com}). By comparing the settling times of the control systems responses in starting regimes with their corresponding settling times in rejection regime of disturbing effects, relatively small differences can be identified. Considering these explanations, the conclusion is that the two proposed control systems from the structure of the proposed control strategy reject with high efficiency the effects of the two considered disturbances which occur simultaneously.

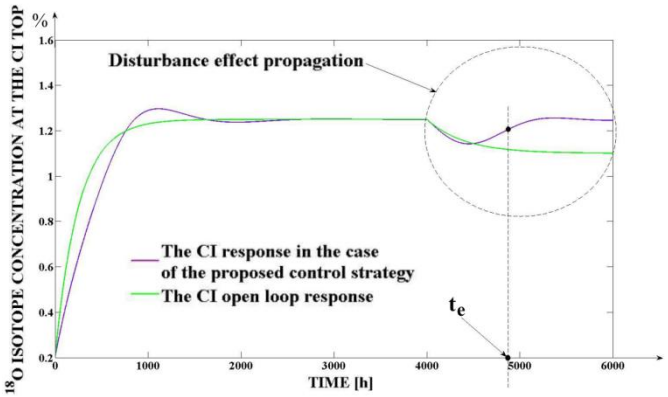

Figure 13. The disturbance effect on the CI operation

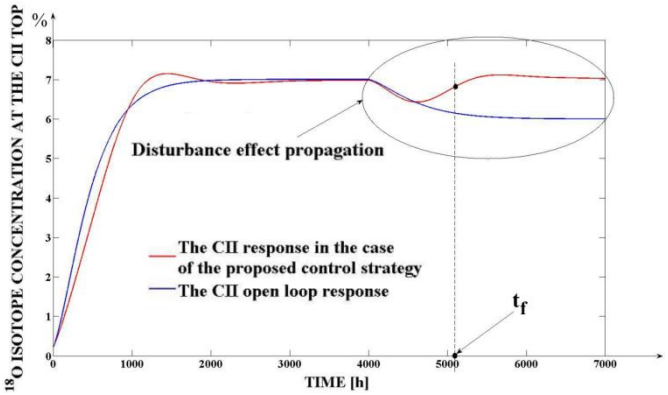

Figure 14. The disturbance effect on the CII operation

The dynamics of the initial control signals $cs_{Ii}(t)$ and $cs_{IIi}(t)$ generated by the two complex controllers CMBCCI and CMBCCII are presented in Fig. 15. The first conclusion which results from Fig. 15 is the fact that the two control signals variation domains are enclosed into the limits of the [2; 10] mA unified current standard, more exactly, both proposed control strategy and the obtained controllers' parameters (after the controllers tuning) are practically feasible.

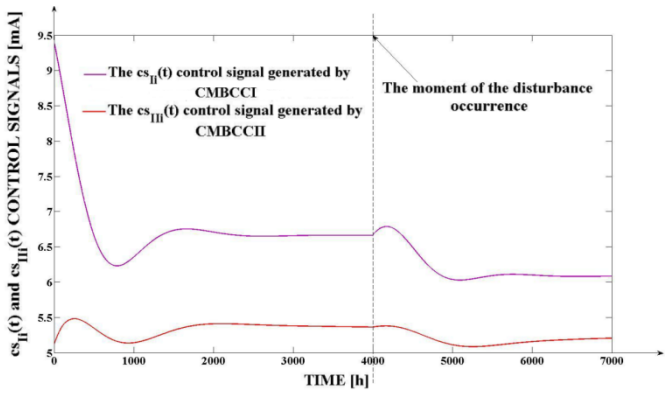

Figure 15. The control signals generated by the two complex controllers CMBCCI and CMBCCII

The control efforts generated by the two complex controllers, in rejection regime, are visible after the moment $t_{com} = 4000$ h through the decrease of the two figured control signals. Immediately after t_{com}, an opposite phenomenon of the two control signals increase can be remarked, having the duration

of several 10^{th} of hours. This phenomenon is due to the dominant effect of the derivative component from the two CMBCC complex controllers' structures. However, this phenomenon, as was previously proven, does not affect significantly the two control systems performances. Also, this phenomenon implies the same type of variation of the signals which are modified as consequence of the $cs_{Ii}(t)$ and $cs_{IIi}(t)$ variations. The decrease of the $cs_{Ii}(t)$ and $cs_{IIi}(t)$ signals after the t_{com} moment highlights the control effort in the regimes of rejecting the effects of the two disturbances because they imply the increase of the $cs_I(t)$ and $cs_{II}(t)$ signals (the $cs_I(t)$ and $cs_{II}(t)$ signals result by subtracting the $cs_{Ii}(t)$ and $cs_{IIi}(t)$ signals from cs_{Imax} and cs_{IImax}).

In Fig. 16, the simulated evolutions, in relation to time, of the two input nitric oxides flows $F_I(t)$ and $F_{II}(t)$ are presented. In order for the dynamics of the two signals to be clearly visible (due to their different magnitudes), $F_I(t)$ is expressed in l/h and $F_{II}(t)$ is expressed in dl/h. Throughout the simulation, the signals from Fig. 16 have opposite monotony compared to the corresponding signals from Fig. 15 since $F_I(t)$ and $F_{II}(t)$ are proportional with $cs_I(t)$ and $cs_{II}(t)$ control signals (not with $cs_{Ii}(t)$ and $cs_{IIi}(t)$). Consequently, the control efforts generated by the CMBCC complex controllers in disturbance rejection regime is visible in Fig. 16, after t_{com} moment, through the increase of the $F_I(t)$ and $F_{II}(t)$ values. The opposite phenomenon of the two flows decrease immediately after t_{com} has the same explanation as the opposite phenomenon of the two $cs_{Ii}(t)$ and $cs_{IIi}(t)$ signals increase immediately after t_{com}.

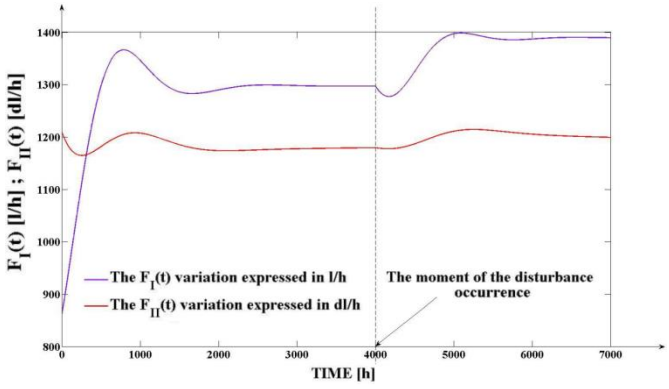

Figure 16. The simulated evolutions, in relation to time, of the FI(t) and FII(t) input nitric oxides flows

$SEP_{II}(t)$ separations are presented in Fig. 17. As it results from Fig. 17, these functions have a similar allure with the $F_I(t)$ and $F_{II}(t)$ signals from Fig. 16. The explanations are as follows: by analysing the $F_I(t)$ and $F_{II}(t)$ values from Fig. 16 in context of Figs. 2 and 4, the fact that in the presented example, only the decreasing linear domains of the two HETP functions are used; consequently, at the increasing of the $F_I(t)$ and $F_{II}(t)$ flows, the HETP functions decrease, respectively at the decreasing of the $F_I(t)$ and $F_{II}(t)$ flows, the HETP functions increase; considering the two separations equations presented in the third section of the manuscript: $SEP_I(t) = \alpha^{\frac{L}{HETP_I(F_I(t))}}$ and $SEP_{II}(t) = \alpha^{\frac{L}{HETP_{II}(F_{II}(t))}}$, the fact that the HETP functions are at the denominator of their exponent can be remarked; consequently, when the HETP functions present an increasing variation, the corresponding separations present a decreasing variation and when the HETP functions present a decreasing variation, the corresponding separations present an increasing variation; considering all these details, at the $F_I(t)$ and $F_{II}(t)$ flows increasing variation, the $SEP_I(t)$ and $SEP_{II}(t)$ functions present, also, an increasing variation, respectively at the $F_I(t)$ and $F_{II}(t)$ flows decreasing variation, the $SEP_I(t)$ and $SEP_{II}(t)$ functions present, also, a decreasing variation. Considering all these details, at the $F_I(t)$ and $F_{II}(t)$ flows increasing variation, the $SEP_I(t)$ and $SEP_{II}(t)$ functions present, also, an increasing variation, respectively at the $F_I(t)$ and $F_{II}(t)$ flows decreasing variation, the $SEP_I(t)$ and $SEP_{II}(t)$ functions present, also, a decreasing variation. Also, in steady state regimes, the $SEP_I(t)$ values are higher than the values of $SEP_{II}(t)$. This aspect occurs since the ratio $\frac{C_{ISP}(t)=1.25\,\%}{C_0} = 6.127$, in case of CI, is higher than the ratio in case of CII, $\frac{C_{IISP}(t)=7\,\%}{C_{ISP}(t)=1.25\,\%} = 5.6$. Obviously, after the t_{com} moment, these separations values are increased due the control effort necessary for rejecting the effects of the two disturbances.

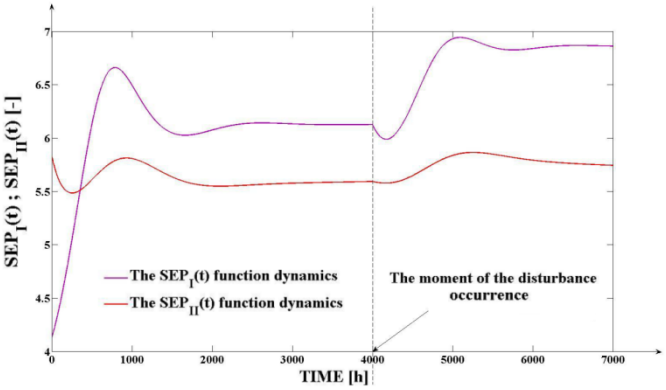

Figure 17. The simulated evolutions, in relation to time, of the $SEP_I(t)$ and $SEP_{II}(t)$ separations

In Fig. 18, the FOCS(t) function variation is highlighted. The usage of FOCS(t) function ensures the correct value of the ^{18}O isotope concentration simulated value at the CII top. In this case, the control effort, in rejection regime of disturbing effects, is visible through the decrease of the FOCS(t) function values.

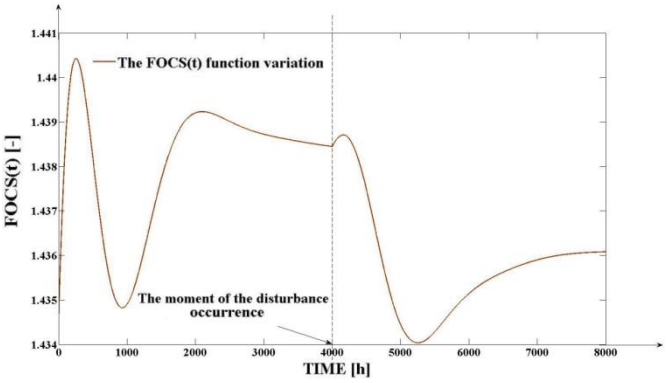

Figure 18. The FOCS(t) compensation signal dynamics

As it is proven in this section of the manuscript, the proposed control strategy is a very effective one in the context in which the addressed separation plant is characterized by multiple and strong nonlinearities.

6. CONCLUSIONS

The manuscript addresses the problem of modelling and controlling the operation of a separation plant, a separation plant used to produce the 18O isotope. The proposed mathematical model that describes the separation cascade operation is an original one and is determined by considering all the nonlinearities of the approached process (without making simplifications, for example linearization type). In this context, it is also considered that the separation process associated with the second separation column (CII) in the cascade separation structure is one of fractional order. The parameters of the mathematical model are identified based on the experimental data obtained from the real plant. The proposed control strategy for controlling the ^{18}O isotope concentration values at the outlets (tops) of the two separation columns (CI and CII) is based on the use of two complex model-based controllers. To be able to implement the nonlinearities of the system, artificial intelligence methods based on neural networks are used. The use of neural networks also provides greater accuracy than using other types of approximations. The efficiency of the proposed solutions (both for modelling and for the control of the separation plant) are proven by the simulations presented in the 5th section of the manuscript. The performance of the control system is successfully tested both in start-up mode and in disturbance rejection mode. In addition to the simulation of the main output signals from the proposed control structure, the simulation of several intermediate signals was also carried out, to highlight some interesting phenomenological aspects regarding the ^{18}O isotope separation technology. As future research directions that can be approached, we can mention: extending the model by also taking into account temperature variations; extending the model to also consider the actual production regime, not just the total reflux regime; extending the control strategy proposed to minimize the energy consumption of the separation plant.

REFERENCES

Abrudean M. (1981*). Isotopic exchange between NO, NO_2 and H_2O, HNO_3, Ph.D. Thesis*, 117. Dept. State Committee for Nuclear Energy, Physics and Nuclear Eng. Institute, Bucharest, Romania;

Axente D., Abrudean M. and Bâldea A. (1994). *15N, 18O, 10B, 13C Isotopes Separation trough Isotopic Exchange*, 189. Science Book House, Cluj-Napoca, România;

Barkan, E. and Luz, B. (2003). High-precision measurements of $^{17}O/^{16o}$ and $^{18}O/^{16}O$ of O_2 and O_2/ Ar ratios in air, Rapid Commun. *Mass Spectrom*., (17), 14;

BrankaTrček, Beno Mesarec (2023). Impact of the Hydroelectric Dam on Aquifer Recharge Processes in the Krško Field and the Vrbina Area: Evidence from Hydrogen and Oxygen Isotopes. *MDPI Mathematics, Water*, (15), 19;

Chen L., Chen, P. and Lin Z. (2020). Artificial Intelligence in Education: A Review. *IEEE Access*, (8), 14;

David Behrens, Jeff B. Langman, Erin S. Brooks, Jan Boll, Kristopher Waynant, James G. Moberly, Jennifer K. Dodd and John W. Dodd (2021). Tracing δ18O and δ2H in Source Waters and Recharge Pathways of a Fractured-Basalt and Interbedded-Sediment Aquifer, Columbia River Flood Basalt Province. *MDPI Mathematics, Geosciences*, (11), 22;

E. R. Th. Kerstel, R. van Trigt, J. Reuss, and H. A. J. Meijer (1999). Simultaneous Determination of the 2H/1H, 17O/16O, and 18O/16O Isotope Abundance Ratios in Water by Means of Laser Spectrometry. *American Chemical Society, ACS Anal. Chem.*, (71), 8;

Hanquan Zhang, Mingming Wen, Yonghang Li, Peng Wan and Chen Chen (2019). High-Precision 13CO2/12CO2 Isotopic Ratio Measurement Using Tunable Diode Laser Absorption Spectroscopy at 4.3 μm for Deep-Sea Natural Gas Hydrate Exploration. *MDPI Mathematics, Appl. Sci.*, (9), 13;

K. A. S. Pathiratne, R. J. Lovett (2016). 6. Isotopes and Atomic Absorption Spectrometry. Computer Simulations, Part I: Evaluation of the Simulation Model Using the Flame Atomic Absorption Determination of Lithium Isotope Abundances. *SAGE Journals*, (41), 10;

Morin S., R. Sander R., and Savarino J. (2011). Simulation of the diurnal variations of the oxygen isotope anomaly (Δ17O) of reactive atmospheric species. *Atmospheric Chemistry and Physics*, (11), 20;

Monje C. A., Chen Y., Vinagre B. M., Xue D., Feliu V. (2010). Fractional-order systems and controls. In Fundamentals and Applications. *Springer*, (3), 9;

Muresan V., Abrudean M., Valean H., Colosi T., Unguresean M., Sita V., Clitan I., Moga D. (2015). Neural modeling and control of a ^{13}C isotope separation process. *In Proceedings of the 12th International Conference on Informatics in Control, Automation and Robotics (ICINCO)*, (12), 9;

Reza Lashkarboluki, Mohammad Hassan Mallah (2022). Process modeling of 18O isotope separation using stochastic exchanges of isotopic components in a packed distillation column. *Scopus, Eurasian Chemical Communications*, (4), 10;

Savarino J. and Morin S. (2011*). Handbook of Environmental Isotope Geochemistry*, Chapter 39. Springer-Verlag, New York, USA.

Savarino J. and Thiemens M. H. (1999). Analytical procedure to determine both $\delta^{18}O$ and $\delta^{17}O$ of H_2O_2 in natural water and first measurements. *Atmosferic Environment*, (33), 7;

Savarino J. and Thiemens M. H. (1999). Mass-independent oxygen isotope (^{16}O, ^{17}O and ^{18}O) fractionation found in Hx, Ox reactions. *The Journal of Physical Chemistry A*, (46), 8;

Wolfram Meier-Augenstein (2017). *Stable Isotope Forensics: Methods and Forensic Applications of Stable Isotope Analysis*, 512. John Wiley & Sons Ltd United Kingdom;